COMPRESSED SENSING BASED INTENSITY NON-UNIFORMITY CORRECTION

Snehashis Roy, Aaron Carass, and Jerry L. Prince

Image Analysis and Communications Laboratory, Electrical and Computer Engineering,
The Johns Hopkins University
{snehashisr,aaron_carass,prince}@jhu.edu

ABSTRACT

We present a compressed sensing based approach to remove gain field from magnetic resonance (MR) images of the human brain. During image acquisition, the inhomogeneity present in the radio-frequency (RF) coil appears as shading artifact in the intensity image. The inhomogeneity poses problem in any automatic algorithm that uses intensity as a feature. It has been shown that at low field strength, the shading can be assumed to be a smooth field that is composed of low frequency components. Thus most inhomogeneity correction algorithms assume some kind of explicit smoothness criteria on the field. This sometimes limits the performance of the algorithms if the actual inhomogeneity is not smooth, which is the case at higher field strength. We describe a model-free, non-parametric patch-based approach that uses compressed sensing for the correction. We show that these features enable our algorithm to perform comparably with a current state of the art method N3 on images acquired at low field, while outperforming N3 when the image has non-smooth inhomogeneity, such as 7T images.

***Index Terms*—** MRI, intensity non-uniformity, intensity inhomogeneity, 7T, bias field, bias correction

1. INTRODUCTION

Several core MR image processing algorithms such as registration and segmentation, use image intensity as a primary feature. Any artifact in the intensities affects the performance of the algorithms severely. Intensity inhomogeneity (IIH) or intensity non-uniformity (INU) is an example of one such artifact. At low magnetic field (1T-3T), this is primarily caused by the presence of non-linear characteristics present in the RF receiver coil. At high field (*e.g.* 7T), this effect is accentuated by the interactions between RF waves and electromagnetic properties of the tissues [1].

Inhomogeneity correction algorithms can be categorized into two primary classes, prospective and retrospective. Prospective methods [2] correct the inhomogeneity by including the imaging equations in the correction methodology, usually by combining multiple images [3, 1] acquired under different parameters. These methods are not applicable to many studies where it is not always possible to acquire multiple images with pre-defined parameters or the acquisition protocols are simply unknown. In contrast, retrospective methods are essentially post-processing methods. They usually assume that the inhomogeneity field is a *smoothly varying non-anatomic multiplicative* field, and is usually written as a linear combination of low order smooth polynomials. Then entropy minimization [4, 5] or deconvolution [6] is used to estimate the smooth IIH field. Often, the correction step is combined with a segmentation algorithm, where simultaneous estimation of tissue classes and inhomogeneity correction can be achieved by a maximum likelihood estimator [7, 8].

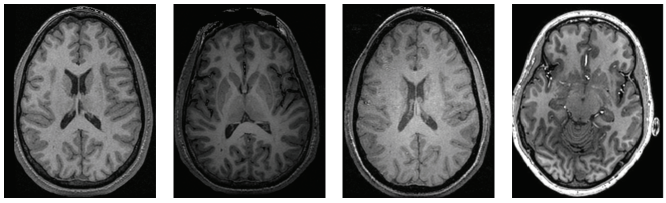

(a) **(b)** **(c)** **(d)**

Fig. 1. A T1 weighted image from **(a)** GE 1.5T scanner, **(b)** Siemens 3T scanner, **(c)** GE 4T scanner [9] and **(d)** Philips 7T scanner.

The smoothness property of the IIH field has been well studied for low field strength. But in high field, the smoothness assumption is often violated. Fig. 1 shows T1-weighted images from a 1.5T, 3T, 4T and 7T scanner, where at 7T, the inhomogeneity is quite different. In this case, a small window of intensity measurements should provide information about the inhomogeneity. This idea is exploited in [10], where a joint entropy minimization framework is described to remove bias from many images simultaneously. In this work, however, we propose a non-parametric compressed sensing based intensity non-uniformity correction (CSI-NC) approach that does not have any explicit smoothness model on the estimated field and does not require many images, thus being more versatile and applicable to situations where the actual IIH is not smooth, e.g. in 7T images.

This work was supported by the NIH/NINDS under grant 5R01NS037747. We would like to thank Emily Wood, Drs. Daniel Reich, Peter Calabresi, Peter van Zijl, and Craig Jones for providing the 7T MR images, which were acquired under Kirby Center's grant NCRR P41 RR15241.

2. METHOD

2.1. Compressed Sensing

We use compressed sensing for our IIH approach. Compressed sensing recovers sparse vectors from their projections onto a set of random vectors [11, 12].

Suppose we want to reconstruct a signal $\mathbf{x} \in \mathbb{R}^d$ which is s-sparse, *i.e.* has at most s non-zero elements. We want to observe another vector $\mathbf{y} \in \mathbb{R}^n$, $n < d$, such that each element of $\mathbf{y}$ can be obtained by an inner product of $\mathbf{x}$ and another vector from $\mathbb{R}^d$. In short, compressed sensing deals with reconstructing $\mathbf{x} \in \mathbb{R}^d$ from $\mathbf{y} \in \mathbb{R}^n$, with $\mathbf{y} = \mathbf{\Phi x}$, $n < d$, $\mathbf{x}$ being s-sparse, $\Phi \in \mathbb{R}^{n \times d}$.

One approach of finding $\mathbf{x}$ is,

$$\hat{\mathbf{x}} = \min ||\mathbf{x}||_0 \text{ such that } ||\mathbf{y} - \mathbf{\Phi x}||_2^2 < \epsilon_1, \tag{1}$$

where ϵ_1 is the noise in the measurement and $|| \cdot ||_0$ indicates the number of non-zero elements in the vector. Although this approach provides simple conditions on $\mathbf{\Phi}$ [13], it is an NP-hard problem. A second approach comes from,

$$\hat{\mathbf{x}} = \min ||\mathbf{x}||_1 \text{ such that } ||\mathbf{y} - \mathbf{\Phi x}||_2^2 < \epsilon_2, \tag{2}$$

where $||\mathbf{x}||_1$ is the L_1 norm of a vector. This is a convex problem and can be transformed into a linear program that can easily be solved. If ϵ_2 is unknown, Eqn. 2 can be written in a more compact form,

$$\hat{\mathbf{x}} = \underset{\mathbf{x}}{\operatorname{argmin}}\{||\mathbf{y} - \mathbf{\Phi x}||_2^2 + \lambda ||\mathbf{x}||_1\}, \tag{3}$$

where λ is a weighing factor. The sparsity on $\hat{\mathbf{x}}$ increases as λ increases.

It has been shown that if $\mathbf{\Phi}$ follows the global restricted isometry property (RIP) [12], then the solutions to Eqn. 1 and Eqn. 2 are identical and the optimal solution can be obtained by such an L_1 minimization problem. This result is interesting because most *random* matrices satisfy the RIP [14]. Thus, to reconstruct $\mathbf{x}$, we have to observe its projections onto a set of random vectors.

2.2. Patch Based Correction

Assume the MR image is partitioned into $p \times q \times r$ patches. If the bias field is not globally smooth, then we can assume that it is at least uniform over a small image patch. Let $d = pqr$, thus each patch can be thought of as a $d \times 1$ vector. Assuming that the gain field is multiplicative, each image patch $\mathbf{y}_k \in \mathbb{R}^d$, $k \in \Omega$, can be written as,

$$\mathbf{y}_k = g_k \mathbf{y}_k^\star + \eta_k, \; g_k > 0 \tag{4}$$

Here, Ω is the image domain, $\mathbf{y}_k^\star$ is the inhomogeneity free image patch, g_k is the bias field for k^{th} location, and η is the image noise. For further analysis, for simplicity we assume that $\eta_k = 0, \forall k$.

The idea behind a patch-matching process is that we want to match $\mathbf{y}_k$ to a set of vectors, called a dictionary, which is given by $\mathbf{\Phi} \in \mathbb{R}^{d \times N}$, such that $\mathbf{y}_k = \mathbf{\Phi x}_k$, $\mathbf{x}_k \in \mathbb{R}^N$, and the high-dimensional sparse vector $\mathbf{x}_k$ carries the information about the multiplicative field g_k.

Intuitively, for a particular $\mathbf{y}_k$, its sparsest representation $\mathbf{x}_k$ from Eqn. 2 is such a vector that $\mathbf{x}_k$ has exactly one non-negative element. That implies $\mathbf{y}_k$ is matched to exactly one vector ϕ from $\mathbf{\Phi}$ by a scaling factor f, ϕ being a column of $\mathbf{\Phi}$. Thus any multiplicative effect on $\mathbf{y}_k$ is reflected on the scaling factor f, which gives a measure of inhomogeneity. In the same context, we follow the idea of the non-negative garrote [15] so that the sparse representations are constrained by $\mathbf{x}_k \geq \mathbf{0}$, to have a meaningful positive weighting of the dictionary $\mathbf{\Phi}$.

Specifically, consider the sparse representations of $\mathbf{y}_k$ and $\mathbf{y}_k^\star$ as $\mathbf{x}_k$ and $\mathbf{x}_k^\star$, respectively. Then Eqn. 3 gives,

$$\hat{\mathbf{x}}_k = \underset{\mathbf{x}}{\operatorname{argmin}}\{||\mathbf{y}_k - \mathbf{\Phi x}||_2^2 + \lambda ||\mathbf{x}||_1\}, \mathbf{x} \geq 0 \tag{5}$$

$$\hat{\mathbf{x}}_k^\star = \underset{\mathbf{x}}{\operatorname{argmin}}\{||\mathbf{y}_k^\star - \mathbf{\Phi x}||_2^2 + \lambda^\star ||\mathbf{x}||_1\}, \mathbf{x} \geq 0 \tag{6}$$

Now if $\mathbf{y}_k = g_k \mathbf{y}_k^\star$, Eqn. 5 gives,

$$\begin{aligned} \hat{\mathbf{x}}_k &= \underset{\mathbf{x}}{\operatorname{argmin}}\{||g_k \mathbf{y}_k^\star - \mathbf{\Phi x}||_2^2 + \lambda ||\mathbf{x}||_1\}, \\ \Rightarrow \hat{\mathbf{x}}_k &= \underset{\mathbf{x}}{\operatorname{argmin}} \left\{ ||\mathbf{y}_k^\star - \mathbf{\Phi} \frac{\mathbf{x}}{g_k}||_2^2 + \frac{\lambda}{g_k} \left|\left| \frac{\mathbf{x}}{g_k} \right|\right|_1 \right\}, \end{aligned} \tag{7}$$

By appropriate conditions on $\mathbf{\Phi}$ as described earlier, and choosing $\lambda = g_k \lambda^\star$, Eqn. 7 and Eqn. 6 give $\hat{\mathbf{x}}_k = \hat{\mathbf{x}}_k^\star g_k$. Thus, an appropriate estimator of g_k is given by,

$$g_k = \frac{||\hat{\mathbf{x}}_k||_1}{||\hat{\mathbf{x}}_k^\star||_1}. \tag{8}$$

2.3. Choice of $\hat{\mathbf{x}}_k^\star$ and $\mathbf{\Phi}$

Eqn. 8 suggests that in an ideal situation, if two inhomogeneity free patches $\hat{\mathbf{y}}_i$ and $\hat{\mathbf{y}}_j$ are of same the tissue and have the same intensity, then $\hat{\mathbf{x}}_i^\star = \hat{\mathbf{x}}_j^\star$ and $g_i \propto ||\hat{\mathbf{x}}_i||_1$, *i.e.*, the L_1 norm of the sparse representation gives the relative amount of gain field for the same tissue.

For a particular k, $\hat{\mathbf{x}}_k^\star$ can be found using a prior information about the tissue classes, which can be obtained from a segmentation of the image. The image being already corrupted with IIH, we only need an approximate segmentation of the image. In our experiments, we have used an atlas based segmentation called TOADS [16] that uses a probability atlas to do the segmentation. We use an approximate segmentation from TOADS, which gives a reasonable segmentation even in the presence of heavy inhomogeneity (*c.f.* Fig. 3(e)). We use 1 iteration of the segmentation algorithm, which provides a hard segmentation image with 4 classes, cerebro-spinal fluid (CSF), gray matter (GM), white matter (WM) and ventricles. For each of the classes, a mean $\mathbf{y}^{(l)}, l = 1, \ldots, 4$ is computed, and their corresponding $\hat{\mathbf{x}}^\star(l)$ are found from Eqn. 5.

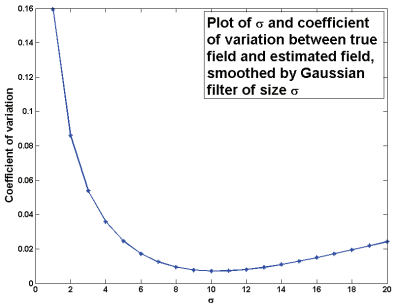

Fig. 2. Plot of σ vs. the coefficient of variation (CV) between the true field and the estimated field, smoothed by a 3D Gaussian filter of size σ. The minimum CV is achieved when $\sigma = 10$mm.

The compressed sensing literature suggests that a good choice of $\mathbf{\Phi}$ is a random matrix. For our experiments, we generate $\mathbf{\Phi}$'s from a uniform distribution once.

The algorithm is described as follows,

1. Partition the image into patches $\mathbf{y}_k,\ k \in \Omega$ of size $p \times q \times r$. In our experiments, $p = q = r = 3$. Generate a random $d \times N$ matrix $\mathbf{\Phi}$. In our experiments, we arbitrarily select $N = 1000$.

2. Find an approximate segmentation of the image using TOADS and compute the mean $\mathbf{y}^{(l)}$'s that represents the l^{th} class, $l = 1, \ldots, 4$. Find the corresponding $\hat{\mathbf{x}}^\star(l)$'s using $\mathbf{\Phi}$ in Eqn. 5.

3. For each k, find the type of the tissue $l_0 \in \{1, \ldots, 4\}$ that $\mathbf{y}_k$ belongs to. If there is more than one tissue type in $\mathbf{y}_k$, we choose the dominant one for simplicity. Then $\hat{\mathbf{x}}_k^\star = \hat{\mathbf{x}}^\star(l_0)$

4. Find the sparse representation of $\mathbf{y}_k$ as $\hat{\mathbf{x}}_k$ from Eqn. 5. We use $\lambda = 0.5$.

5. Find the gain field g_k using $\hat{\mathbf{x}}_k$ and $\hat{\mathbf{x}}^\star(l_0)$ using Eqn. 8.

Here we note that all images are normalized, so that their WM peaks have the same value. The final inhomogeneity field becomes blocky because there is no explicit smoothness criterion on the image model. As a post-processing step, we smooth the field by a Gaussian filter with size σ, that we estimate based on phantom validation, described in the next section. The filter also smooths out bad estimates of $\hat{\mathbf{x}}_k$'s near the tissue boundaries.

3. RESULTS

3.1. Phantom Validation

We compare CSI-NC with a current state of the art method called non-parametric non-uniform intensity normalization (N3) [6], which tries to restore the corrupt image by a histogram deconvolution assuming the field is smooth. We use a phantom image from Brainweb [17] database, for which

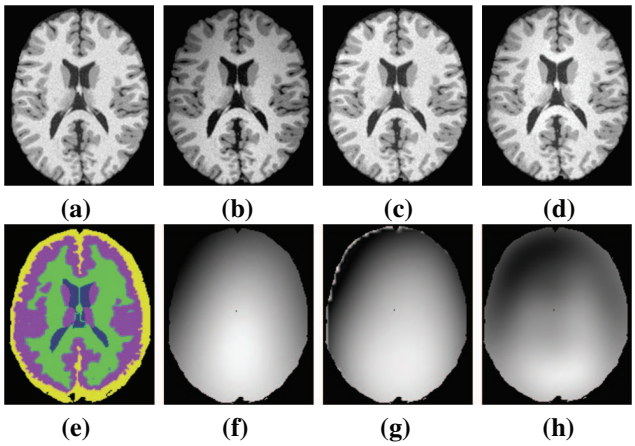

Fig. 3. **(a)** Original inhomogeneity free image, **(b)** corrupted by 20% INU as described in [17], **(c)** N3 corrected image, **(d)** CSI-NC corrected image, **(e)** crude segmentation by TOADS [16] that is used to find $\hat{\mathbf{x}}^\star(l)$ described in Sec. 2.3, **(f)** true inhomogeneity field "C", **(g)** N3 inhomogeneity field, **(h)** CSI-NC field, smoothed by a Gaussian filter of size $\sigma = 10$mm.

the inhomogeneity field is known (referred to as "field C" on [17]). The final inhomogeneity field is smoothed by a 3D Gaussian filter of size σ, chosen such that the coefficient of variation (CV) of the estimated smooth field and true field is minimum. CV is defined as $C = \frac{\sigma(B_e/B_a)}{\mu(B_e/B_a)}$, where B_e and B_a are the estimated and the applied field and it measures how much the estimated field differs from the true field in a normalized way. Fig. 2 shows the plot of σ vs the CV. The minimum CV$= 0.01$ is attained at $\sigma = 10$mm. The magnitude of the CV is comparable to that reported earlier [4]. The original and corrected images and the corresponding fields are shown in Fig. 3.

3.2. Experiment on 7T images

As Brainweb phantoms have very smooth inhomogeneity, it is very difficult to see the improvement of CSI-NC over other methods. It is explicitly seen when the inhomogeneity is not smooth. In those cases, the polynomial based algorithms will not perform better simply by increasing the degree of polynomials because the coefficients can not be estimated in a robust fashion in a high-dimensional parameter space. Instead, we employ a patch based method. We use both CSI-NC and N3 on Philips 7T MPRAGE (magnetization prepared rapid gradient echo) and FLAIR (fluid attenuated inversion recovery) images, $256 \times 320 \times 320$ volumes, 0.70mm isotropic.

As we don't have any ground truth to compare the inhomogeneity fields, we visually compare the results from the two algorithms. Fig. 4 shows a 7T FLAIR image and its correction by both N3 and CSI-NC. As N3 assumes some underlying smoothness criterion on the inhomogeneity field, it can not remove the localized IIH present in the CSF at the

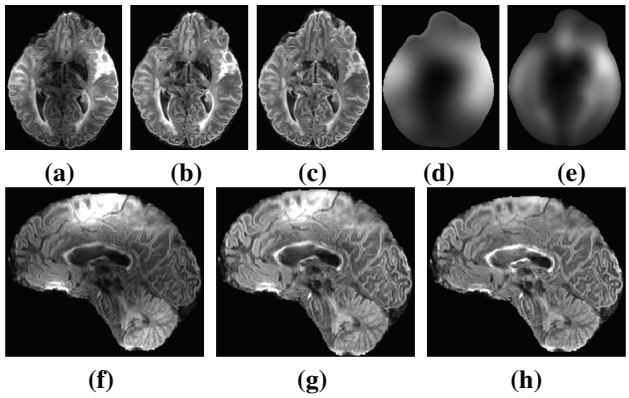

Fig. 4. **(a)** Original 7T FLAIR image, **(b)** N3 corrected FLAIR, **(c)** CSI-NC corrected image, **(d)** N3 field, **(e)** smoothed field from CSI-NC, smoothed by Gaussian filter of size 10mm, **(f)** a sagittal view of the original FLAIR, **(g)** sagittal view of N3 corrected image, **(h)** sagittal view of CSI-NC corrected image. As N3 assumes an underlying smoothness model on the inhomogeneity, small localized inhomogeneity that are present in small tissue structures are not corrected.

superior part of the brain (Fig. 4(g)), while CSI-NC, being a patch-based method, corrects the bias in that area (Fig. 4(h)).

We also use one 7T MPRAGE image to test the effectiveness of our algorithm. In the absense of a ground truth, we visualize the inner cortical surfaces, generated using a geometric deformable model based surface reconstuction algorithm [18]. Fig. 5(a) shows the original MPRAGE image, showing large inhomogeneity near the anterior and posterior parts of the brain. Its correction by N3 and CSI-NC are shown in Figs. 5(a)-(b). A zoomed view of the anterior part shows that inner surface is pushed outwards deep inside GM on N3 corrected image, while it respects the WM-GM contrast in the CSI-NC corrected image.

4. SUMMARY AND CONCLUSION

We have presented a patch based intensity inhomogeneity correction method that uses the concept of compressed sensing. Our method is non-parametric, model-free and does not impose any smoothness constraint on the field. We have shown that our method works better on 7T images, at least visually, compared to N3, although there is some over-correction visible near the peri-ventricular region, where the method needs improvement. Future work includes estimation of optimal size λ, N and size of patches. We would also validate the method on 7T images.

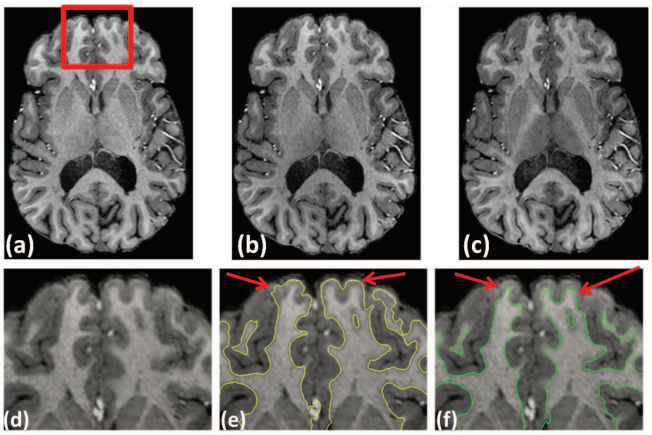

Fig. 5. **(a)** Original 7T MPRAGE image, **(b)** correction by N3, **(c)** correction by CSI-NC, **(d)** a zoomed in version of the original MPRAGE, **(e)** inner cortical surface [18] generated from the N3 corrected image (yellow) and **(f)** from CSI-NC corrected image (green), overlaid on the original MPRAGE.

5. REFERENCES

[1] P.-F. Van de Moortele *et. al.*, "T1 weighted Brain Images at 7 Tesla Unbiased for Proton Density, T2* contrast and RF Coil Receive B1 Sensitivity with Simultaneous Vessel Visualization," *Neuroimage*, vol. 46, no. 2, pp. 432–446, 2009.

[2] L. Axel *et. al.*, "Intensity correction in surface-coil MR imaging," *American Journal Roentgenol*, vol. 148, no. 2, pp. 418–420, 1987.

[3] H. Mihara *et. al.*, "A method of RF inhomogeneity correction in MR imaging," *Mag. Res. Materials in Phy., Bio. and Med.*, vol. 7, no. 2, pp. 115–120, 1998.

[4] J. V. Manjon *et. al.*, "A nonparametric MRI inhomogeneity correction method," *Med. Image. Anal.*, vol. 11, no. 4, pp. 336–345, March 2007.

[5] J. F. Mangin *et. al.*, "Entropy Minimization for Automatic Correction of Intensity Nonuniformity," in *IEEE Workshop on Math. Methods in Biomed. Image Anal.*, June 2000, pp. 162–169.

[6] J. G. Sled *et. al.*, "A non-parametric method for automatic correction of intensity non-uniformity in MRI data," *IEEE Trans. on Med. Imag.*, vol. 17, no. 1, pp. 87–97, 1998.

[7] M. Styner *et. al.*, "Parametric Estimate of Intensity Inhomogeneities applied to MRI," *IEEE Trans. on Med. Imag.*, vol. 19, no. 3, pp. 153–165, 2000.

[8] K. Van Leemput *et. al.*, "Automated Model-Based Tnumber Classification of MR Images of the Brain," *IEEE Trans. on Med. Imag.*, vol. 18, no. 10, pp. 897–908, 1999.

[9] L. Friedman *et. al.*, "Test-Retest and Between-Site Reliability in a Multicenter fMRI Study," *Human Brain Mapping*, vol. 29, no. 8, pp. 958–972, August 2008.

[10] E. Learned-Miller and V. Jain, "Many heads are better than one: Jointly removing bias from multiple MRs using nonparametric maximum likelihood," in *Proc. Inf. Proc. in Med. Imag. (IPMI)*, 2005, pp. 615–626.

[11] D. L. Donoho, "Compressed sensing," *IEEE Trans. Inf. Theory*, vol. 52, no. 4, pp. 1289–1306, April 2006.

[12] E. J. Candes *et. al.*, "Stable signal recovery from incomplete and inaccurate measurements," *Comm. on Pure and Appl. Math.*, vol. 59, no. 8, pp. 1207–1223, August 2006.

[13] M. Elad and A. M. Bruckstein, "A Generalized Uncertainty Principle and Sparse Representation in Pairs of Bases," *IEEE Trans. Inf. Theory*, vol. 48, no. 9, pp. 2558–2567, September 2002.

[14] R. Baraniuk *et. al.*, "A simple proof of the restricted isometry property for random matrices," *Constructive Approximation*, vol. 2008, 2007.

[15] L. Breiman, "A Generalized Uncertainty Principle and Sparse Representation in Pairs of Bases," *Technometrics*, vol. 37, no. 4, pp. 373–384, November 1995.

[16] P. L. Bazin and D. L. Pham, "Topology-preserving tissue classification of magnetic resonance brain images.," *IEEE Trans. Med. Imaging*, vol. 26, no. 4, pp. 487–496, April 2007.

[17] C. A. Cocosco *et. al.*, "Adaptive Fuzzy Segmentation of Magnetic Resonance Images," *NeuroImage*, vol. 5, no. 4, pp. S425, 1997.

[18] X. Han *et. al.*, "CRUISE: Cortical Reconstruction Using Implicit Surface Evolution," *NeuroImage*, vol. 23, no. 3, pp. 997–1012, 2004.